IOPscience iopscience.iop.org

Home Search Collections Journals About Contact us My IOPscience

Radially selective inward transport of positrons in a Penning–Malmberg trap

This content has been downloaded from IOPscience. Please scroll down to see the full text.

2014 New J. Phys. 16 073028

(http://iopscience.iop.org/1367-2630/16/7/073028)

View the table of contents for this issue, or go to the journal homepage for more

Download details:

IP Address: 137.44.14.61
This content was downloaded on 18/07/2014 at 07:30

Please note that terms and conditions apply.

New Journal of Physics
The open access journal at the forefront of physics
Deutsche Physikalische Gesellschaft DPG | IOP Institute of Physics

Radially selective inward transport of positrons in a Penning–Malmberg trap

A Deller[1], T Mortensen[2], C A Isaac, D P van der Werf and M Charlton
Department of Physics, College of Science, Swansea University, Singleton Park, Swansea SA2 8PP, UK
E-mail: a.deller@ucl.ac.uk

Received 12 January 2014, revised 9 June 2014
Accepted for publication 11 June 2014
Published 17 July 2014
New Journal of Physics **16** (2014) 073028
doi:10.1088/1367-2630/16/7/073028

Abstract
The anharmonic component of the electric field of a Penning–Malmberg trap is exploited to manipulate a subset of the radial (r) distribution of trapped positrons, using a dipole field made to rotate about the long-axis (z) of the trap. This 'rotating wall' technique (RW) induces inward transport at frequencies associated with the motion of trapped particles, although similarly it causes heating. The motional frequencies vary spatially within a non-ideal trap, thus resonant interaction with the rotating field may be restricted to a region selected to lie away from the trap centre, thereby forming a pseudo-potential barrier and reducing losses due to both heating and expansion. We demonstrate this effect for improved accumulation of positrons and further outline a technique to achieve strong compression with low RW amplitudes by chirping the drive frequency.

Keywords: antimatter, positrons, Penning traps, rotating wall

1. Introduction

Low energy positron beams have applications across a number of areas of atomic and condensed matter physics (see e.g., [1–3] for overviews), and have been combined with devices

[1] Present address: University College London, Gower Street, London WC1E 6BT, UK
[2] Present address: IRFU/ CEA, Saclay, F-91191 Gif-sur-Yvette Cedex, France

Content from this work may be used under the terms of the Creative Commons Attribution 3.0 licence. Any further distribution of this work must maintain attribution to the author(s) and the title of the work, journal citation and DOI.

© 2014 IOP Publishing Ltd and Deutsche Physikalische Gesellschaft

for accumulating and storing positrons in electromagnetic traps [4]. These traps use a series of appropriately biassed electrodes to create an electric trapping potential along the z-axis of the system, in combination with an axial magnetic field ($\mathbf{B} = B\hat{\mathbf{z}}$) to provide radial confinement, and typically employ low density buffer gas(es) to capture and cool the antiparticles. Such devices are examples of Penning, or Penning–Malmberg, traps: an instrument found throughout experimental physics and chemistry, with applications too numerous to mention here. Positron traps have been used in scattering and annihilation investigations (reviews can be found in [5, 6]), in studies of positronium and its molecule [7–10] and in the creation, trapping and study of antihydrogen [11–19].

The behaviour of charged particles in ideal Penning traps is well documented (see e.g., [20]) and only a summary of the aspects most relevant to this study is given here. In a uniform magnetic field, and in the absence of an electric field, charged particles (of charge q and mass m) radially precess in orbits at the cyclotron frequency, $\omega_c = qB/m$. However, when the Penning electric trapping potential is applied $\mathbf{E} \times \mathbf{B}$ effects give rise to superimposed radial trajectories in which: (i) ω_c is modified to ω_+, and (ii) the particle exhibits magnetron motion with a frequency ω_-. These frequencies are given by,

$$\omega_\pm = \frac{1}{2}\left(\omega_c \pm \sqrt{\omega_c^2 - 2\omega_z^2}\right), \tag{1}$$

where ω_z is the axial bounce frequency, which is dependent upon the electrode geometry and the applied voltages. We emphasize that for non-ideal traps (e.g., positron accumulators) this frequency will vary depending on the energy and location of a given particle, although it is approximately constant for low energies and near axial positioning. For the trap parameters used in these studies the three frequencies are estimated to be $\omega_+ \approx 5.8$ Grad s^{-1}, $\omega_z \approx 58$ Mrad s^{-1} and $\omega_- \approx 290$ krad s^{-1}.

Positron accumulators commonly feature devices that can be used to tailor the radial properties of the particle distribution using the so-called rotating wall (RW) technique. A rotating electric field applied using a segmented electrode in the vicinity of the trapped particles is used to counteract the plasma/cloud expansion, or to actively compress it. A significant motivation for the development of techniques to manipulate positron plasmas is to provide bright sources of the antiparticles, which can further be time-compressed to produce narrow time-width pulses, e.g. for recapture in antihydrogen experiments [12, 13, 21] and to provide dense positronium clouds [7–10].

When the particle motion within a cloud is dominated by the trapping fields, such is classified as being in the single-particle regime. If the particles are at sufficiently low temperatures and high densities that the self-electric fields strongly influence their motion, they are said to form a non-neutral plasma. The RW technique has been applied in both the plasma (see e.g., [22–25]) and single-particle [26–29] cases. To avoid significant losses, the heating that the rotating electric field induces must be countered. In high magnetic fields ($\gtrsim$1 T) cyclotron radiation is usually sufficient, however in traps with lower fields a suitable cooling gas (e.g., SF_6or CF_4) is introduced [30, 31].

In the absence of a rotating field the trapped positron lifetime is foremost limited by radial transport to the electrode walls, expedited by collisions with the background gases used for capture and cooling. These losses are virtually eliminated by application of the RW technique [30], however depletion of the antiparticles due to their annihilation with the requisite gases is unavoidable; thus optimum yields are found through careful tuning of their partial pressures. In

these studies the loss rate as a consequence of diffusion is estimated to be $3\,s^{-1}$, in comparision to an estimated $0.5\,s^{-1}$ due to annihilations on a 10^{-4} mbar nitrogen background.

This article will focus on positron clouds in the single-particle regime, and in particular we build upon the work of Isaac and co-workers [27–29] who studied a sideband ($\omega_z \pm \omega_-$) excitation technique to compress positron clouds held in a two-stage accumulator [32]. The authors employed an asymmetric rotating dipolar electric field that deactivated the lower sideband, as such facilitating shrinkage of the magnetron motion (compression) across a range of frequencies centred at $\omega_0 = \omega_z + \omega_-$. Cooling of the axial motion was provided by gas collisions and modelled using a Stokes viscous drag approximation with a characteristic friction coefficient, κ. Isaac *et al* [27, 28] showed that the particles undergo RW compression at a drive frequency ω_r and exponentially approach the trap axis with a characteristic rate, Γ, given by

$$\Gamma = \frac{\kappa}{4}\left(1 - \sqrt{\frac{(\omega_r - \omega_0)^2}{\delta^2 + (\omega_r - \omega_0)^2}}\right), \tag{2}$$

where the width of the cusp, δ, is dependent on the applied rotating wall amplitude, a, (see [27]) via

$$\delta = \frac{a}{\sqrt{(\omega_+ - \omega_-)\,\omega_z}}. \tag{3}$$

Optimum compression rates close to 10^3 s^{-1} were reported, and found to be linearly dependent upon the RW amplitude, in agreement with equation (3). Thus, and with widths in the range 50–100 kHz, significant compression was shown.

The above model is here used to explain the effect of a RW employed throughout positron accumulation across a range of drive parameters, by extending it to the non-ideal features of the trap potential (section 3.2). We further demonstrate that the anharmonicity of the trap can be actively exploited to selectively address particles with the RW, in such a way as to inhibit expansion to the electrode walls yet minimise losses due to heating, and thereby improving the overall accumulation yield.

2. Non-ideal traps

The ideal Penning trap employs a ring electrode and two hyperbolic end-cap electrodes to produce an harmonic electric potential. The Penning–Malmberg variant [33] is instead comprised of three coaxial, cylindrical electrodes that lie parallel to the magnetic field lines, along which charged particles can easily be loaded into the trap. The simple concept is readily extendible to more complex configurations (e.g. positron accumulators and nested traps [34]), however it can only approximately reproduce the harmonic potential of the ideal case.

For particles held in non-ideal traps the triplet of Penning frequencies ($\omega_\pm$, ω_z) are broadened to spectra, the breadth of which correspond to the degree of anharmonicity in the trap potential and the distribution in phase-space of the trapped particles. Similarly to the ideal case, the three motions are entwined, thus the effect of anharmonicities may be quantified by resolving the structure in any one of them.

Recently we developed a technique to manipulate the radial position at which accumulated clouds are ejected from the trap [29]. By applying a pulsed dipole field with a segmented electrode, an offset radial orbit of the cloud could be precisely controlled. After removal of the

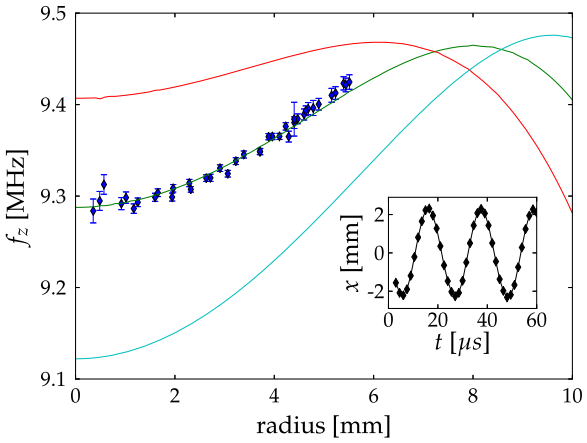

Figure 1. The axial bounce frequency ($f_z = \omega_z/2\pi$) as a function of radial position (points), derived from measurements of ω_-—see text. Calculations (lines) of f_z for positrons displaced from the trap centre with kinetic energies of 100 meV (red), 400 meV (green) and 700 meV (cyan). Inset: an example magnetron orbit of an 0.8 mm (FWHM) positron cloud, used to determine ω_-.

field the clouds maintain coherent magnetron orbits about the trap centre. These orbits were tracked by varying the time prior to ejection of the cloud, then fitting a 2D Gaussian to its image at an micro-channel plate (MCP) (see section 3.1). An example of the x position of a cloud during a typical magnetron orbit is given in the inset of figure 1; these data can be fitted to find ω_-, through which we observe that the frequency varies with the orbit radius. This results from a shift to ω_z as the cloud samples increasingly anharmonic regions of the trapping potential.

Using the fitted result for ω_- the corresponding value of ω_z can be obtained from equation (1). The main panel of figure 1 shows the variation of the derived ω_z against the radial position of the orbit, exhibiting a systematic increase of around 1.4% as the radius increases out to just over 5 mm. Also given in figure 1 are the results of calculations of ω_z for positrons with axial kinetic energies of 100, 400 and 700 meV, as displaced from the centre of the trap. The line at 400 meV most closely matches the measured variation with r. The calculated frequencies were found by integrating the time of an axial bounce in a computationally derived model of the electric potential well. Note: the error-bars in figure 1 do not include the uncertainty in ω_c, which was fine-tuned in the calculations to bring ω_z into the expected region.

Both the calculations and measurements indicate that the frequency of resonant compression ($\omega_z + \omega_-$) will shift upwards for the off-axis positrons, which together with the natural width of the compression curve (which, as shown in equation (3), is also proportional to the applied RW amplitude via the parameter a) will produce significant, strongly amplitude-dependent compression effects far from the on-axis resonance frequency.

3. Positron accumulation

3.1. Apparatus

Our two-stage positron accumulator [32] uses nitrogen buffer gas to promote capture and cooling of positrons into a Penning–Malmberg trap. The positrons are accumulated in the second stage of the trap, a region with a gas pressure in the range 10^{-4}–10^{-5} mbar. A schematic of the second stage

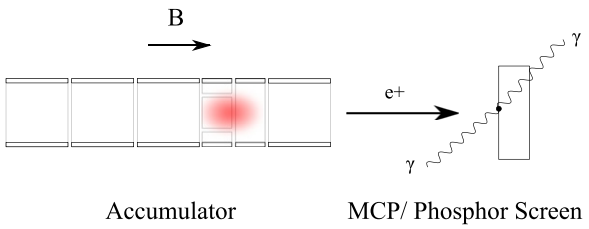

Figure 2. Schematic illustration of the second stage accumulation region and electrodes, and the segmented electrode used for RW compression. The positron clouds (red) are ejected from the trap and imaged using the MCP/phosphor screen assembly, which is viewed by an external CCD camera. The gamma-rays are detected by a CsI scintillation counter (not shown). The accumulator is immersed in a magnetic field of around 33 mT, produced by an external solenoid.

electrodes and the detection system used to diagnose the properties of the trapped cloud is shown in figure 2. The electrodes which make up the second stage are each 49 mm in length and have an internal diameter of 41 mm: these are aligned parallel to the ~33 mT field of the encasing solenoid. As shown in figure 2, one of these electrodes is split into two, with one half segmented into four arcs. It is this electrode that is used to apply a rotating dipole electric field to the cloud by biassing the segments with $\pi/2$ phase-shifted sinusoidal voltages.

After 1s of accumulation on the order of 10^5 positrons are collected in the second stage, fed by a low energy positron beamline. Use of the RW during accumulation (see below) requires the presence of an extra cooling gas, to counteract the positron heating caused by the rotating electric field. In our case SF_6 is used, as this is known to be an efficient positron cooler (e.g., [35]).

3.2. Accumulation with RW

Positrons were accumulated for 1 s with a RW signal applied continuously throughout, following which the cloud was rapidly ejected from the trap and the number of particles and the radial profile determined [30]. The former was found using an external CsI gamma-ray detector for which the annihilation signal was normalized to that obtained without the RW and with the SF_6 partial pressure in the accumulation/ compression region estimated to be 9×10^{-6} mbar. The radial profile was determined by imaging with a CCD camera the MCP and phosphor screen arrangement depicted in figure 2. The measurements were repeated for a range of RW parameters (frequency/ amplitude) and with a number of different cooling gas pressures.

Figure 3 shows the number of positrons accumulated with low cooling gas pressure (9×10^{-6} mbar) versus RW frequency ($f_r = \omega_r/2\pi$) for various applied voltages (V_r). We identify the dip feature which is present, and accentuated at the higher amplitudes, to be due to loss of positrons at, or close to, the on-axis resonance frequency $f_0 = \omega_0/2\pi \approx 9.3$ MHz. We attribute this loss to heating of the cloud by the rotating field, and note that the positron loss mechanisms of radial expansion to the electrode walls and positronium formation with the background gases [36, 37], will both be enhanced by such.

At the lowest RW amplitude there is insufficient power far below resonance to counteract the collision-driven expansion of the positrons, and there is no increase in accumulated number. Nor is there a significant increase at f_0, where the off-axis particles feel little compressive force and are lost to expansion. The maximum response occurs around 180 kHz above this point,

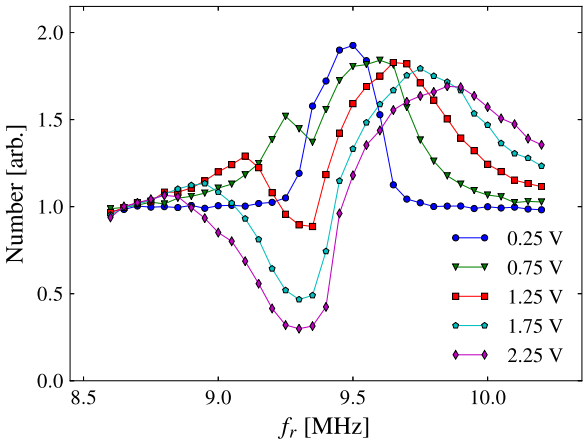

Figure 3. The number of accumulated positrons versus the RW frequency at various amplitudes, V_r; the cooling gas partial pressure is ~9×10^{-6} mbar. The scale is arbitrary, but normalized against accumulation without RW.

where the RW induces inward transport of those positrons which are off-axis by several mm, thus inhibiting those at smaller radii from expanding to the electrodes (i.e. the RW creates a pseudo-potential barrier which prevents anything inside from escaping, yet causes minimal heating to the particles trapped inside). As the frequency is increased further past resonance, the compressive force is insufficient to counteract expansion and the accumulated signal drops. It is interesting to note that, at these pressures, the maximum yield of trapped positrons is achieved at this low RW voltage and is around a factor of two higher than can be attained by accumulating without the RW (for this example of a 1 s accumulation cycle). At these settings the clouds are not particularly small (FWHM ~5 mm), yet further manipulations can obtain denser clouds, as will be described in section 3.3.

For the largest RW amplitude losses at f_0 are clearly apparent, whilst the remainder of the frequency profile reflects competition between heating and reduced radial expansion. The interim amplitudes combine features of the two extremes in proportional measure. They indicate that loss (i.e. heating) correlates with amplitude, and affirm the expected link between amplitude and response width (equation 3). This is reflected in the maximum yield frequency, which is found invariably above the on-axis resonance frequency and shifted by an amount that increases linearly with V_r.

Figure 4 (a, b) shows the accumulated positron number versus RW frequency for various SF_6 cooling gas pressures at fixed values of V_r of 0.5 and 2 V, respectively. For increasing SF_6 pressure the number of positrons is generally observed to decrease: as discussed previously, this is dominated by collision-induced diffusion to electrodes—at least for those frequencies at which the RW is inactive. The vertical bands of enhanced accumulation (centred ~9.5 MHz), are attributed to the frequency ranges in which the RW induces inward transport, with now the losses at the higher pressures predominantly a result of annihilations with the gas molecules.

With $V_r = 0.5$ V the enhancement band is restricted to a narrow range centred above f_0. The relatively weak inward transport produced at this amplitude is only effective by way of preventing off-axis particles from drifting to the wall; this feature is similar to the peaked structure in figure 3 at $V_r = 0.25$ V. In contrast, with $V_r = 2.0$ V the increased width of the compression curve (equation 3) is reflected by the broad range of frequencies found to improve

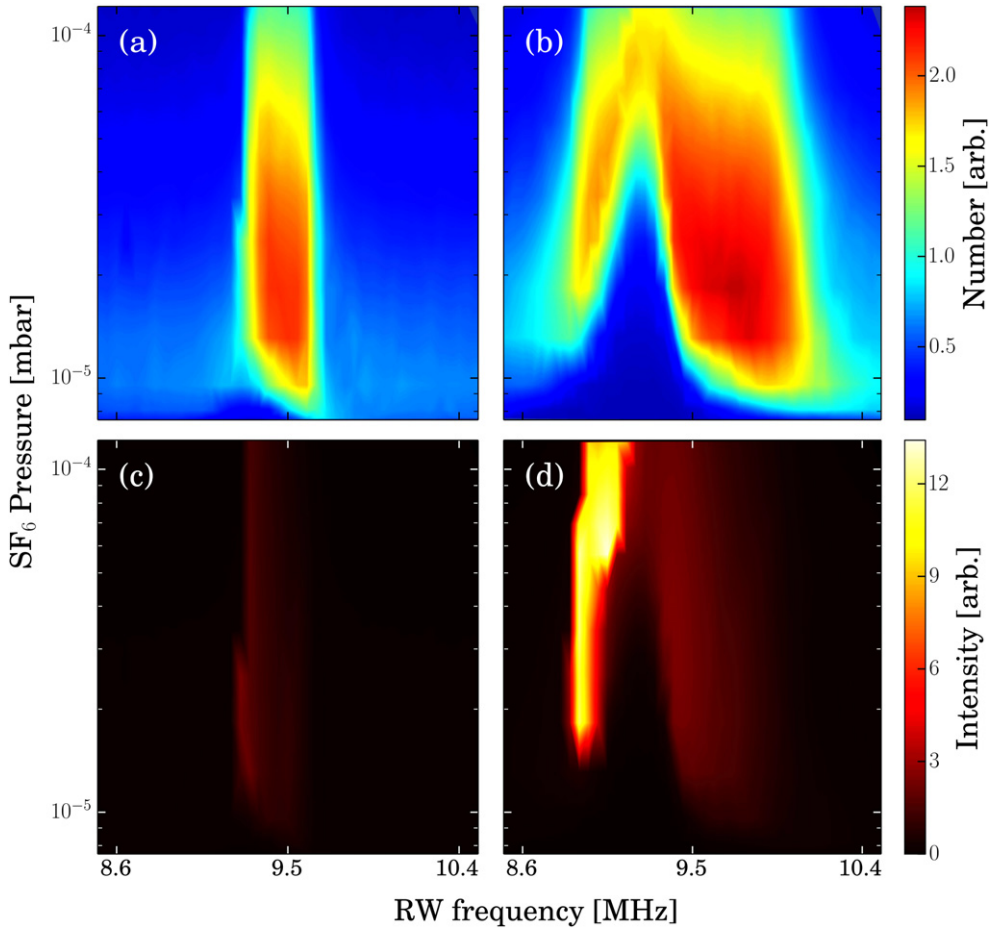

Figure 4. The number (a, b) and peak CCD intensity (c, d) for positrons imaged after 1 s accumulation, with various cooling gas pressures (log scale). The RW is applied throughout, and the measurements made across a range of RW frequencies and with the amplitude fixed at either 0.5 V (a, c) or 2 V (b, d).

accumulation. Prominent at this higher amplitude is the loss feature centred around f_0. Detuning both above and below the axial resonance value provides an increase in accumulation yield comparable to the use of the weaker field.

We note that figures 3 and 4 (a), (b) all indicate a range of RW drive parameters for which the accumulated number is close to the maximum observed. For certain applications other features, such as the cloud size/ density, are of additional interest. Imaging the clouds and recording the peak intensity on the CCD gives an indication of the cloud density—figures 4 (c), (d). This shows that the densest clouds are found for the larger RW amplitude and at frequencies less than and near to f_0 (accordingly significant cooling gas must be present). Compression is perhaps strongest here as a result of the cusp profile of the compression function. By tuning below resonance, heating is lessened to those on axis, which are compressed as if a weaker field is resonantly applied; unlike such, the broad wings of the cusp will yet address particles at both larger radii and higher energies (lower f_0—see figure 1), inhibiting their expansion and driving them towards the centre. The total number attainable with

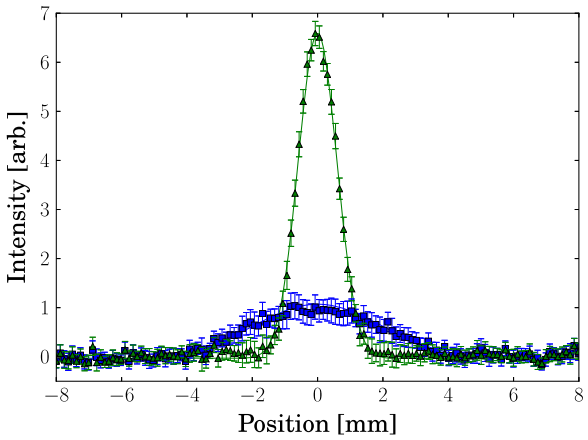

Figure 5. Radial profiles of the positron clouds imaged by the CCD after accumulation with $V_r = 0.5$ V and $f_r = 9.45$ MHz (■), followed by an 150 ms linear chirp to 9.1 MHz (▲). The lines show Gaussian fits to the data.

this configuration is however slightly less than when optimally accumulating above resonance, due to increased heating on axis.

3.3. Frequency chirped RW

Based upon the measurements above, a scheme was devised to attain higher output densities with a low drive amplitude. Accumulation for 1 s with the RW optimally tuned for total number was followed by a frequency chirp applied to the drive that swept the compressive force inward through the trap radii, prior to ejecting the cloud. For a RW amplitude of 0.5 V this was found to result in a seven fold increase in areal density; the optimum result was found by chirping from 9.45 MHz to 9.10 MHz in 150 ms (see figure 5). We might expect to find the optimal end-frequency to be the presumed on axis resonance frequency (9.3 MHz), yet it was found to be somewhat less. This is perhaps indicative of heating of the cloud by the chirp technique (for 700 meV positrons f_0 is reduced to ∼9.1 MHz—figure 1). The total number is however unaffected by the frequency chirp, suggesting any heating to be quite moderate. Note that these clouds are enlarged by a factor of 2.7 over their size in the accumulator, due to the lower magnetic field at the MCP.

Although the chirped clouds are substantially denser than could be attained with a static frequency 0.5 V RW, they are yet 60% the maximum areal density observed with the 2.0 V RW drive (figure 4(d)). Nonetheless, the enervated need for cooling gas with this low amplitude scheme would be advantageous for longer accumulation cycles, for which the lifetime due to annihilation on the background gases would be of greater significance for the final yield.

4. Conclusions

In summary, RW compression phenomena are observed and qualitatively explained by extrapolating the expected behaviour in an ideal system [27, 28], to the known perturbations of our anharmonic trap. This allows us to selectively address a subset of the trapped positrons, in a manner analogous to other pseudo-potential manipulations, such as magneto-optical trapping. We demonstrate that the broadband sideband compression method of Isaac and co-workers

[27–29] can be employed to enhance the accumulated yields in a Penning–Malmberg trap. Furthermore, the clouds accumulated with a low amplitude RW can then be efficiently compressed to form bright output beams using a frequency chirp method. These techniques are simple to implement and could be exploited widely in experiments requiring spatially focussed low energy positron beams.

Acknowledgments

We thank the EPSRC for its support, currently via award EP/H026932/1 and for studentship support for AD and TM. DPvdW thanks the Leverhulme Trust for Research Fellowship award RF-2012-495. We are grateful to the technical staff of the Physics Department at Swansea University for their enthusiastic support.

References

[1] Coleman P (ed) 1999 *Positron Beams and their Applications* (Singapore: World Scientific)
[2] Dupasquier A and Mills Jr A P (ed) 1995 Positron Spectroscopy of Solids *Proc. Int. School of Physics 'Enrico Fermi': Course CXXV* (Amsterdam: IOS Press)
[3] Charlton M and Humberston J W 2001 *Positron Physics* (Cambridge: Cambridge University Press)
[4] Murphy T J and Surko C M 1992 *Phys. Rev.* A **46** 5696
[5] Surko C M, Gribakin G F and Buckman S J 2005 *J. Phys.* B **38** R57
[6] Gribakin G F, Young J A and Surko C M 2010 *Rev. Mod. Phys.* **82** 2557
[7] Cassidy D B and Mills A P Jr 2007 *Nature* **449** 195
[8] Cassidy D B, Hisakado T H, Tom H W K and Mills A P Jr 2012 *Phys. Rev. Lett.* **108** 043401
[9] Cassidy D B, Hisakado T H, Tom H W K and Mills A P Jr 2012 *Phys. Rev. Lett.* **108** 133402
[10] Cassidy D B, Hisakado T H, Tom H W K and Mills A P Jr 2012 *Phys. Rev. Lett.* **109** 073401
[11] Amoretti M *et al* 2002 *Nature* **419** 456
[12] Jørgensen L V *et al* 2005 *Phys. Rev. Lett.* **95** 025002
[13] Funakoshi R *et al* 2007 *Phys. Rev.* A **76** 012713
[14] Enomoto Y *et al* 2010 *Phys. Rev. Lett.* **105** 243401
[15] Andresen G B *et al* 2010 *Nature* **468** 673
[16] Andresen G B *et al* 2011 *Nat. Phys.* **7** 558
[17] Amole C *et al* 2012 *Nature* **483** 439
[18] Amole C *et al* 2013 *Nat. Commun.* **4** 1785
[19] Gabrielse G *et al* 2012 *Phys. Rev. Lett.* **108** 113002
[20] Brown L S and Gabrielse G 1986 *Rev. Mod. Phys.* **58** 233
[21] Comeau D *et al* 2012 *New J. Phys.* **14** 045006
[22] Anderegg F, Hollmann E M and Driscoll C F 1998 *Phys. Rev. Lett.* **81** 4875
[23] Greaves R G and Surko C M 2000 *Phys. Rev. Lett.* **85** 1883
[24] Danielson J R and Surko C M 2005 *Phys. Rev. Lett.* **94** 035001
[25] Danielson J R, Surko C M and O'Neil T M 2007 *Phys. Rev. Lett.* **99** 135005
[26] Greaves R G and Moxom J M 2008 *Phys. Plasmas* **15** 072304
[27] Isaac C A, Baker C J, Mortensen T, van der Werf D P and Charlton M 2011 *Phys. Rev. Lett.* **107** 033201
[28] Isaac C A 2013 *Phys. Rev.* A **87** 043415
[29] Mortensen T, Deller A, Isaac C A, van der Werf D P, Charlton M and Machacek J R 2013 *Phys. Plasmas* **20** 012124

[30] van der Werf D P, Isaac C A, Baker C J, Mortensen T, Kerrigan S J and Charlton M 2012 *New J. Phys.* **14** 075022
[31] Bertsche W and Fajans J 2003 *Non-Neutral Plasma Physics V* **692** 235
[32] Clarke J, van der Werf D P, Griffiths B, Beddows D C S, Charlton M, Telle H H and Watkeys P R 2006 *Rev. Sci. Instrum.* **77** 063302
[33] Malmberg J H and Driscoll C F 1980 *Phys. Rev. Lett.* **44** 654
[34] Quint W, Kaiser R, Hall D and Gabrielse G 1993 *Hyperfine Interact.* **76** 181
[35] Al-Qaradawi I, Charlton M, Borozan I and Whitehead R 2000 *J. Phys.* B **33** 2725
[36] Marder S, Hughes V W, Wu C S and Bennett W 1956 *Phys. Rev.* **103** 1258
[37] Obenshain F E and Page L A 1962 *Phys. Rev.* **125** 573